

# Synthesis of Bioactive Chemicals Cross-linked Sodium Tripolyphosphate (TPP) - Chitosan Nanoparticles for Enhanced Cytotoxic Activity against Human Ovarian Cancer cell Line (PA-1)

Sujima Anbu A<sup>1</sup>, Sahi SV<sup>2</sup> and Venkatachalam P<sup>1,2\*</sup>

<sup>1</sup>Plant Genetic Engineering and Molecular Biology Lab, Department of Biotechnology, Periyar University, Periyar Palkalai Nagar, Salem-636011, Tamil Nadu, India

<sup>2</sup>Department of Biology, Western Kentucky University, Bowling Green, KY 42101-1080, USA

## Abstract

Currently, nanotechnology makes an impact in all spheres of human life and creates increasing excitement especially in the field of biomedicine and bionanotechnology. The important symbiosis between nanotechnology and green chemistry is the use of bioactive chemicals for the synthesis of nanoparticles. The present research was focused on fabrication of biomolecules loaded chitosan nanoparticles using *Gymnema sylvestre* leaf extract (GSCNPs). The experiment was performed using ionic gelation technique and was characterized using FTIR, TEM, XRD, Zeta potential and pdi. The morphological investigation showed the presence of smooth spherical surfaced GSCNPs with 58-80 nm in size. The XRD results indicated the crystalline nature of the synthesized nanoparticles. The FTIR results showed the absorption peaks stretching from higher wavelength region to lower region demonstrating the interaction of tripolyphosphate with chitosan and biomolecules. The zeta potential revealed the positive surface charges proving the stability of the synthesized nanoparticles and homogeneous dispersion was presented by the polydispersity index. The cytotoxic activity was performed against PA-1 cell line and the IC<sub>50</sub> values obtained were 931 µg/ml for *G. sylvestre* leaf extract (GSLE) and 378.4 µg/ml for GSCNPs respectively. The present study strongly suggested that the fabricated phytochemicals cross-linked chitosan nanoparticles from *Gymnema sylvestre* leaf extracts exhibited enhanced cytotoxic activity and it could be effectively used as a promising anticancer agent in the near future.

**Keywords:** Chitosan; Cytotoxicity; *Gymnema sylvestre*; Nanoparticles; Ovarian cancer; Phytochemicals

## Introduction

Cancer begins when cells in part of our body start to grow out of control. Ovarian cancer is the leading cause of death from gynecological malignancy [1]. Despite recent advances in research and treatment options, the 5-year overall survival rate exists around 47% while 50% ends in mortality when affected with this cancer [2]. Clinicians recognize ovarian cancer as a set of heterogeneous diseases though it is treated as a single disease using a combination of debulking surgery and platinum-based chemotherapy. Established cell lines provide a valuable tool for studying biological functions at the molecular and cellular level. The advantage of high proliferative capacity, clonogenicity and extended life span exists in the human ovarian cancer cell lines today [3]. Since the recurring tumor growth as poor diagnostic indicator and additional line of chemotherapy failure occurs, there is a need for development of new effective anti-cancer drug in the case of ovarian cancer [4]. Thus there is need for development of new anti-cancer drug which could be derived from herbs for treatment of ovarian cancer.

The chemical, toxicological and pharmacological features of plants have been investigated by the researchers with the presence of active phytochemicals [5,6]. *Gymnema sylvestre* R. Br. is an important medicinal plant species that possess various phytochemicals like alkaloids, terpenoids, phenolics, steroids and flavonoids in different quantities. Gymnemic acid from *Gymnema* plant has been proved to possess hypocholesterolemic property and is responsible for central nervous system activities [7]. The insulin modulating activity of this plant and *Gymnema* is proved to be one of the most significant herbs in the treatment of the underlying factor of insulin resistance, amenorrhea, hirsutism, hormonal balance and infertility associated with polycystic ovary syndrome (PCOS) [8]. Insulin resistance is implicated in the etiology of PCOS through insulin's stimulation of ovarian androgen production and reduction of hepatic synthesis of sex

hormone-binding globulin [9]. Adverse condition of the syndrome leads to metabolic disorders such as type 2 diabetes, cardiovascular diseases and gynaecological cancers in the affected women populations.

There is a need to investigate the potential phytochemical based nanoparticle that has been prompted due to the dramatic expansion of the nanotechnology. Due to their unique size, the nanoparticles tend to own novel physical, chemical and biological properties that make these nanomaterials superior in the field of nanomedicine [10]. Thus, 'green chemistry' that uses plant biomass or plant extracts have become an alternative for the production of nanomaterials in a clean, non-toxic, eco-friendly and sustainable manner [11]. The world's second most abundant biopolymer, the chitosan, is a cationic polysaccharide which is obtained by partial deacetylation of chitin. The amine and -OH groups endow chitosan with many special properties, making it applicable in many areas and easily available for chemical reactions [12]. Natural chitosan material has attracted great attention in pharmaceutical and biomedical fields because of its advantageous functional properties. Recently, chitosan has paid a great attention in pharmaceutical and biomedical research due to its several advantages: a) biocompatible, biodegradable with non-toxicity polysaccharide, b) easy movement

**\*Corresponding author:** Venkatachalam P, Professor, Department of Biotechnology, Periyar University, Periyar Palkalai Nagar, Salem-636011, Tamil Nadu, India, Tel: 0427-2345766; Fax: 0427-2345124; E-mail: [pvenkat67@yahoo.com](mailto:pvenkat67@yahoo.com)

**Received** December 16, 2016; **Accepted** December 22, 2016; **Published** December 31, 2016

**Citation:** Sujima Anbu A, Sahi SV, Venkatachalam P (2016) Synthesis of Bioactive Chemicals Cross-linked Sodium Tripolyphosphate (TPP) - Chitosan Nanoparticles for Enhanced Cytotoxic Activity against Human Ovarian Cancer cell Line (PA-1). J Nanomed Nanotechnol 7: 418. doi: [10.4172/2157-7439.1000418](https://doi.org/10.4172/2157-7439.1000418)

**Copyright:** © 2016 Sujima Anbu A, et al. This is an open-access article distributed under the terms of the Creative Commons Attribution License, which permits unrestricted use, distribution, and reproduction in any medium, provided the original author and source are credited.

across cell membrane, c) efficient protection of drugs till reaching the target, d) releasing the drug in controlled manner and e) degradation of the carrier molecule upon drug delivery and most of the features are rapidly applied to delivery drugs, wound healing, antimicrobial and antioxidant properties, anti-inflammatory, antiulcerogenic and anticancer activity. The positive charge of chitosan is responsible for enhanced drug absorption by cells. [13-18]. In addition, chitosan acts as excellent moisturizing agent due to its water retention capacity. It also provides absorption promoting effect that prolongs the contact time between substrate and cell membrane [19]. In view of the above, the present study was focused on fabrication and characterization of biomolecules cross-linked with chitosan nanoparticles using *G. sylvestre* plant leaf extracts and to determine its cytotoxic potential against the human ovarian cancer cell line (PA-1).

## Materials and Methods

### Preparation of plant extract

The plant extract was prepared from the leaves of *Gymnema sylvestre* R. Br. The leaf materials were collected from Periyar University Campus, Salem. The dust particles on the leaf surface were removed by washing under tap water, shade dried for 10 days and made into fine powder. The coarse powder of *G. sylvestre* [100 g (w/v)] was extracted with 500 ml of hydro-methanol (20:80) using soxhlet apparatus for 12 h at 64°C not exceeding the boiling point of the solvents. The extract was then concentrated to dryness and used for further experimental analysis.

### Synthesis of chitosan nanoparticles

The ionic-gelation method was employed for the synthesis of chitosan nanoparticles using sodium tripolyphosphate (TPP) as cross-linking agent. About 1.5% (w/v) of the plant extract was mixed with 0.5% (w/v) of TPP and the solution was added drop wise using syringe into the chitosan solution containing 1% (w/v) chitosan and 2% (v/v) acetic acid under gentle magnetic stirring. After the formation of opalescent suspension, the sample was centrifuged at 8000 rpm for 20 mins. The resulting pellet was sonicated, dried and used for characterization.

### Characterization of nanoparticles

**FTIR spectral analysis:** After sonication, the biomolecules loaded chitosan nanoparticles were freeze-dried and the powdered sample was used for FTIR spectroscopy studies (Perkin Elmer Make-Model spectrum RX). The dried experimental sample was directly placed on the potassium bromide crystals and was compressed to form pellets. The FTIR spectrum peaks were absorbed in the transmittance mode and recorded in the spectral region from 4000  $\text{cm}^{-1}$  to 400  $\text{cm}^{-1}$ .

**XRD measurements:** The physical form of drug dispersion with chitosan matrix of nanoparticles was studied using X-ray diffraction. The synthesis of chitosan nanoparticles was confirmed by XRD. The synthesized nanoparticle solution was drop coated onto a glass substrate and carried out on Shimadzu-model XRD6000, operated at a voltage of 40 kV and a current of 30 mA with Cu, K $\alpha$  radiation in a 2 $\theta$  configuration from 10-60° and the diffraction pattern of the synthesized nanoparticles was obtained.

**Transmission electron microscopy (TEM) analysis:** The structure and the size of the synthesized nanoparticles were determined using Transmission Electron Microscopy (TEM) analysis (Philips make model Technai 10). The samples were stained with 2% phosphotungstic

acid for 30 s and placed on copper grids for viewing the nanoparticles at 200-1000 nm. The image of the nanoparticles surface was recorded with a high-energy beam of electrons in a pattern of raster scan.

**Zeta potential determinations:** The zeta potential and particle size distribution were measured using the Malvern Zetasizer Instrument Ltd, based on Dynamic Light Scattering technique. The stability of the synthesized nanoparticle was measured by detecting the surface charge at a scattering angle of 90 degrees at 25°C after dissolving the particles in distilled water. The size distribution in liquids was evaluated using the photon correlation spectroscopy method. The samples were measured in triplicate and presented as Mean  $\pm$  Standard deviation.

**Polydispersity index examinations:** The dispersion homogeneity of the synthesized nanoparticles is the measure of polydispersity index (pdi) that ranges from 0 to 1. The homogeneity is indicated by values closer to 0 (zero) and heterogeneity is indicated by values greater than 0.5. The data readings were performed at 25°C after placing the samples in the analyser chamber with a detected angle of 90°.

### Determination of *in vitro* cytotoxicity of the synthesized nanoparticles

**Cell culture and maintenance:** Human ovarian cancer cell lines (PA-1) and Mouse embryo cell lines (3T3) were purchased from National Center for Cell Science (NCCS, Pune). The cells were cultured 75-cm<sup>2</sup> flask containing Dulbecco's modified Eagle's medium (DMEM; Sigma) and the medium was supplemented with 10% Fetal bovine Serum (FBS; Invitrogen), 1.5 g/L sodium bicarbonate (Gibco), 10,000 U/ml penicillin (Gibco), 10 mg/ml streptomycin (Gibco) and 25  $\mu\text{g}/\text{ml}$  Amphotericin B (Gibco). Cells were cultured as monolayers in culture flasks at 37°C under a humidified atmosphere of 5% CO<sub>2</sub> in air. All experiments were performed using cells from passage 20 or less. During the experiment time, the serum containing medium was replaced by serum free medium containing 2-2.5  $\mu\text{g}/\text{ml}$  of the crude, which were dissolved in DMSO and the stock maintained in -20°C. The final working concentration of DMSO was less than 1.0%. The cells reaching 80-90% of confluence were trypsinized and used for subculture. The medium from the culture flask was aspirated; cells were rinsed with 2 ml of PBS and aspirated quickly and 0.5 ml of trypsin-EDTA (0.5% trypsin, 5.3 mM EDTA sodium salt) solution was added and incubated at room temperature (in the laminar hood) for 30-60 sec. Then the trypsin-EDTA solution was aspirated quickly and the flask was incubated in CO<sub>2</sub> incubator for 2 min and tapped gently at the bottom for complete detachment of cells from the surface of the flask. The cells were then gently re-suspended in fresh growth medium and transferred to sterile 75 cm<sup>2</sup> flasks and the total volume was made up to 20 ml with growth medium.

**Cell viability and cytotoxicity determination:** The viability of cultured cells was assessed by MTT assay [20]. The cells were plated separately in 96 well plates at a concentration of  $1 \times 10^5$  cells/well. After 24 h, cells were washed twice with 100  $\mu\text{l}$  of serum-free medium and starved for an hour at 37°C. After starvation, cells were treated with different concentrations of plant extract [(GSLE) 250-1000  $\mu\text{g}/\text{ml}$ ] and the synthesized biomolecules loaded chitosan nanoparticle (GSCNPs) 100-400  $\mu\text{g}/\text{ml}$  for 48 h. At the end of the treatment period, the medium was aspirated and serum free medium containing MTT [3-(4,5-dimethylthiazol-2-yl)-2,5-diphenyltetrazolium bromide] (0.5 mg/ml) was added and incubated for 4 h at 37°C in a CO<sub>2</sub> incubator. The 50% inhibitory concentration dose (IC<sub>50</sub>) of the crude extracts as well as nanoparticles was identified in cancer cell lines. The MTT containing medium was then discarded and the cells were washed with PBS (200

µl). The crystals were then dissolved by adding 100 µl of DMSO and it was mixed thoroughly and used for spectrophotometry analysis. The absorbance of the purple blue formazan dye was measured in a microplate reader at 570 nm (Biorad 680). Cytotoxicity was determined using Graph pad prism5 software.

**Measurement of caspase-9 activity:** The caspase-9 assay delivers a simple and suitable method for quantifying the enzyme activity of caspases. The activity of Caspase-9 was measured in PA-1 cells treated with GSLE and GSCNPs. After incubation for 24 hours, the cells were digested with cell lysis buffer and supernatant was coated on to a 96 well plate with the addition of 100 µl of primary antibody to each well obtained from Invitrogen, USA. The entire set up was incubated at room temperature for 2 hours. The unbound detection antibody was removed then by the wash step and 100 µl (1:1000) of the secondary antibody, Horse Radish Peroxidase (HRP) was finally added that was obtained from Santa Cruz, USA. Using the Danisidine- H<sub>2</sub>O<sub>2</sub> substrate, the color was developed and optical density was measured using an ELISA reader at 410 nm. The concentration of caspase-9 in the samples was then determined by comparing the Optical Density of the samples to the Standard Curve.

**Assessment of DNA damage by comet assay:** Single cell gel electrophoresis (SCGE) or the comet assay is a sensitive method, well-established for detecting single/ double-strand DNA breaks, DNA cross-links, base/ base-pair damages, alkali labile sites, and apoptotic nuclei. The assay was performed according to the method of Dhawan et al. [21]. Briefly, PA-1 cells were cultured and treated with GSLE and GSCNPs at different concentrations (50-200 µg/ml) in 6 well plates. After incubation, the cells were trypsinized, washed and used for comet assay. The fully frosted microscope slides after pre-coating with 1 ml of 0.75% (w/v) normal melting point agarose (NMA Invitrogen, USA), were stored at 4°C. This layer was removed before use and NMA (used 120 µl of 0.75%) was pipetted on to the slides, which were then covered with cover slips. Low melting point agarose (10 µl, Invitrogen, USA) were mixed with the cell suspensions (1 × 10<sup>4</sup>/5-10 µl) and pipetted over the first layer of agarose. NMA (80 µl) was used as a final protective layer. The slides were incubated at 4°C for 10 mins for allowing the agarose to set. The cold lysing solution consisted of 2.5 M NaCl, 100 mM Na<sub>2</sub>EDTA, 10 mM Trizma base, pH 10 and 1% (w/v) SDS to which 10% (v/v) DMSO and 1% (w/v) Triton X- 100 were prepared and added to the slides immediately prior to use for 1 hr. Then the slides were placed in electrophoresis buffer (300 mM NaOH and 1 mM Na<sub>2</sub>EDTA, pH 13) after lysis for 20 min to allow unwinding of DNA. In the same buffer, the electrophoresis was conducted by applying an electric current of 0.8 V/cm (300 mA) for 20 m using an electrophoresis supply. Finally the slides were washed in neutralization buffer (0.4 µL Tris-HCl, pH 7.5) for three times with 5 min each, dried and then stained with 50 µl ethidium bromide (20 µg/ml). FPG (formamidopyrimidine - DNA glycosylase), an endonuclease with specific activity towards oxidized purine was used for the detection of oxidative damage. Then the slides were washed with enzyme reaction buffer (40 mM HEPES, 0.1 M KCl, 0.5 mM Na<sub>2</sub>EDTA, 0.2 mg/ml BSA, pH 10 ) and incubated with ether buffer of 50 µl concentration or FPG in buffer (50 µl, 1 mg/ml FPG) at 37°C for 30 mins for DNA unwinding leading to completion of electrophoresis. The slides were washed in neutralizing buffer (0.4 mM Tris-HCl, pH 7.5) three times finally for five minutes, dried and then stained with 50 µl of ethidium bromide (20 µg/ml) for 15 minutes and then washed with PBS to remove the excess EtBr. The slides were placed under inverted epifluorescent microscope Olympus CKX41 attached with Opitka Pro5 CCD camera to capture the images and comets were

scored using Tritex comet scoring software. Finally the results were statistically correlated.

**Statistical analysis:** All the observed data were statistically analysed. One-way ANOVA with Dunnett's post-test using GraphPad, InStat and Prism version 3.00 for Windows, GraphPad Software, San Diego, CA, USA were used for significant interpretation.

## Results and Discussion

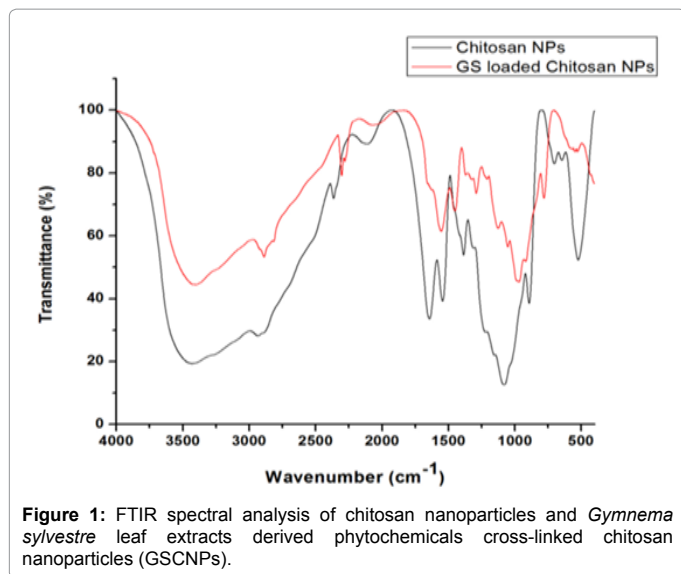
### Fabrication of nanoparticles

In the present study, the *G. sylvestre* plant extract was prepared using methanol as the solvent in the ratio of 20:80 using soxhlet apparatus. The nanoparticles were synthesized by adding sodium tripolyphosphate (0.5% w/v) mixed with *G. sylvestre* plant extract (1.5% w/v) drop wise to the chitosan solution (1% w/v) under constant stirring at pH value of 5.5. The ionic gelation process was employed for the synthesis of chitosan nanoparticles due to their mild and simple protocol [22]. The mechanism behind is the physical cross linking of chitosan with the multivalent anions derived from sodium tripolyphosphate [23]. The properties such as the quick gelling ability and non-toxicity nature makes the TPP favourable cross-linker for ionic gelation. The pH value of the reaction medium has a significant role for the formation of nanoparticles. It influences the positive charge to neutralize with the gradual de-protonation of ammonium groups aiding in the formation of smaller nanoparticles. The pKa value of chitosan (~6.5) is found in the amino group that leads to protonation in acidic to neutral solution with a charge density dependent on pH. This property makes chitosan water- soluble and increases its nature of bioadhesivity [24]. The synthesized nanoparticles were found to be more stable and did not get affected by any temperature. Similar results were obtained from the study of Swarnalatha et al. [16] where alkaloid loaded chitosan nanoparticles were synthesized to determine its anticancer effect against A549 cell lines.

The synthesized nanoparticles were used for further characterization. Earlier report indicated that when TPP was used as anionic cross-linker for chitosan nanoparticles preparation, the particles were homogeneous, and possess positive surface charge that make them suitable for mucosal adhesion applications [25].

### Characterization of the synthesized nanoparticles

**FTIR spectral analysis:** The capability of the ionic gelation process to form biomolecules loaded chitosan nanoparticles was assessed by FTIR for the determination of plant-chitosan interactions. FTIR measurements were carried out to identify the possible biomolecules responsible for chitosan nanoparticle formation. The spectral analysis of chitosan nanoparticles and bioactive molecules loaded chitosan nanoparticles are depicted in the Figure 1. The IR studies of chitosan nanoparticles (CNPs) revealed the presence of peaks at 3430 cm<sup>-1</sup>, 2933 cm<sup>-1</sup>, 2364 cm<sup>-1</sup>, 1642 cm<sup>-1</sup>, 1543 cm<sup>-1</sup>, 1385 cm<sup>-1</sup>, 1081 cm<sup>-1</sup>, 891 cm<sup>-1</sup>, 645 cm<sup>-1</sup> and 522 cm<sup>-1</sup> while the FTIR spectra of *Gymnema sylvestre* plant extract derived chitosan nanoparticles (GSCNPs) showed strong absorption peaks at 3423 cm<sup>-1</sup>, 2924 cm<sup>-1</sup>, 2360 cm<sup>-1</sup>, 1638 cm<sup>-1</sup>, 1539 cm<sup>-1</sup>, 1385 cm<sup>-1</sup>, 1074 cm<sup>-1</sup> and 883 cm<sup>-1</sup>. The spectra observed at 3423 cm<sup>-1</sup> for the synthesized nanoparticle indicates the stretching of O-H bonds indicating reduced hydrogen bonding. The occurrence of reduced hydrogen bonding in the cross-linked nanoparticles complexes was due to more open structure resulting from cross linking with saponin biomolecules of *Gymnema sylvestre* as well as TPP. The peaks recorded at 2924 cm<sup>-1</sup> represents the C-H stretch of the alkanes group. The strong band noticed at 2360 cm<sup>-1</sup> indicates the presence



of phosphorous groups. This might be due to the tripolyphosphoric group linking of TPP with ammonium group of chitosan. The isolated alkene groups of the C=C stretch was found at  $1638\text{ cm}^{-1}$  for the biomolecules loaded chitosan nanoparticles. The absorption spectra observed at  $1539\text{ cm}^{-1}$ ,  $1528\text{ cm}^{-1}$  and  $1539\text{ cm}^{-1}$  indicated the presence of carboxylate group. The bands obtained at  $1385\text{ cm}^{-1}$  and  $1383\text{ cm}^{-1}$  represents the  $-\text{NO}_2$  (aliphatic) nitro groups stretching. The C-N stretching of aliphatic amines was observed at the peaks of  $1074\text{ cm}^{-1}$  and the aromatic groups were presented with intense peaks at  $883\text{ cm}^{-1}$  for the synthesized nanoparticles. These observed peaks were shifted from the higher wave number region to the lower wave number region due to the interaction of the tripolyphosphate molecules binding with chitosan and the plant bioactive molecules. Due to the increase in the bond length, the stretching frequency has decreased and the wave numbers have shifted from higher frequency to lower frequency. Thus it is found that the inter- and intra-molecular actions are enhanced in chitosan nanoparticles. Similar results were also recorded by Rejinold et al. [26] also reported the shifts from the higher frequency to the lower frequency for saponin loaded chitosan nanoparticles. The present results are in agreement with earlier report [27].

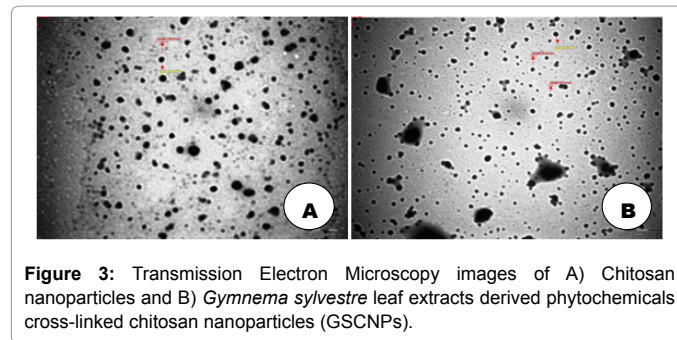
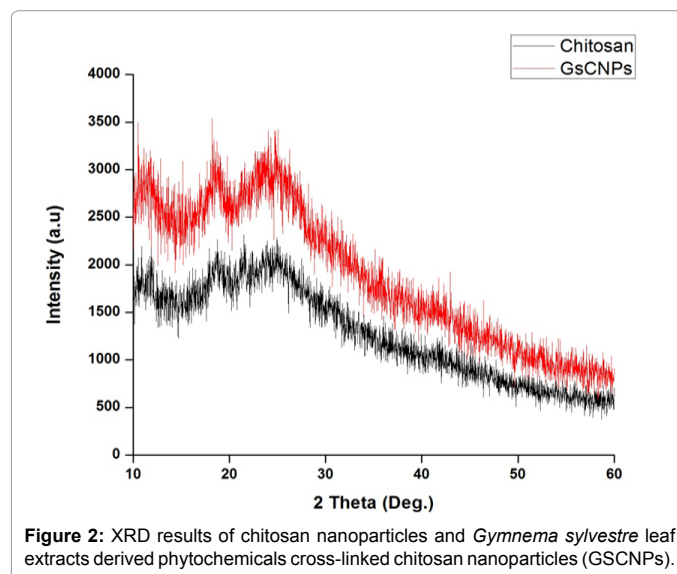
**XRD measurements:** The X-Ray diffraction pattern of the synthesized chitosan nanoparticles and GSCNPs is presented in Figure 2. The formation of chitosan nanoparticles was confirmed by XRD analysis and the measurement was carried out using XRD analyzer. The average particle size of the chitosan as well as the biomolecules loaded chitosan nanoparticles by the green synthesis method was calculated by using Debye-Scherrer Equation,  $D = K\lambda/\beta \cos\theta$ , where  $D$  = the crystalline size of chitosan nanoparticles,  $\lambda$  = the wave length of x-ray source ( $0.1541\text{ nm}$ ) used in XRD,  $\beta$  = the full width at half maximum of the diffraction peak,  $K$  = the Scherrer constant with value from 0.9 to 1,  $\theta$  = the Bragg angle [28]. The chitosan nanoparticles showed intense peaks at  $14.93^\circ$ ,  $25.00^\circ$ ,  $28.95^\circ$ ,  $30.49^\circ$ ,  $36.28^\circ$ ,  $43.79^\circ$  and  $65.65^\circ$ . Chitosan nanoparticles consist of a dense network structure of interpenetrating polymer chains crosslinked to each other by TPP.

The XRD pattern for the *Gymnema sylvestre* biomolecules loaded chitosan nanoparticles showed different peaks at  $18.21^\circ$ ,  $25.03^\circ$ ,  $28.19^\circ$ ,  $35.12^\circ$ ,  $43.00^\circ$  and  $46.47^\circ$ . The XRD result exhibited greater disarray in chain alignment in the nanoparticles after crosslinks due to the change in the chitosan-TPP-GS leaf extract packing structure. These shifts of

the absorption peaks confirmed the crystalline nature of the synthesized chitosan and biomolecules loaded chitosan nanoparticles. It is finally recognized that the width of X-ray diffraction peak is related to the size of the crystallite and the appearance of broadened peaks are the result from imperfect crystal [27-28]. Similar results were also observed with chitosan and chitosan-ZnO nanoparticles by AbdElhady et al. [26].

**TEM analysis:** The morphology and size of the nanoparticle predicted by TEM analysis showed in the Figure 3. According to the TEM image, the chitosan nanoparticles were found to be spherical in shape with smooth surface (Figure 3A). The morphological structure of the biomolecules loaded green synthesized chitosan nanoparticles (GSCNPs) indicated that they were almost spherical in shape with smooth surface (Figure 3B). The size of the chitosan nanoparticles was ranged from 53.11 to 81.82 nm whereas the size of the GSCNPs was between 58-80 nm. Similar results were also obtained by Elsayed et al. [29] who attempted to deliver oral insulin using chitosan-sodium lauryl sulfate as a carrier system. Avadi et al. [30] also reported that chitosan coated insulin nanoparticles were found to be oval and spherical shape with smooth surfaces. The comprehensive properties of the synthesized nanoparticles are illustrated briefly in Table 1.

**Zeta potential determinations:** The stability of suspension and adhesion of particles onto the biomolecule surface was determined by a critical parameter known as the surface charge. Zeta potential plays an important role in the nanoparticle characterization which is dependent on the polyelectrolyte ratio. The results for the zeta potential measurements of both chitosan nanoparticles and chitosan



bioactive molecules coated chitosan nanoparticles (GSCNPs) are depicted in Figure 4. The chitosan nanoparticles obtained were found to be positively charged with values of +2.39 mV, while the GSCNPs expressed higher zeta potential with more stability (+3.25 mV) compared to the chitosan nanoparticles. This may be attributed to the fact that the positive charges on the nanoparticles might be responsible for the cellular membrane components and the tight junctions that could trigger the cellular permeation [31]. The stability of nanoparticles is influenced by the cross-linkers used in the synthesis process. The TPP used in the present study for the biofabrication of nanoparticles is the most widely used cross-linkers that possess anionic and non-toxicity nature [32]. The surface charge determination is explained by the particle formation mechanism where the positively charged amine groups are neutralized by their interaction with the negative charge in tripolyphosphate molecules. The amino group residues would be responsible for the positive potential [30]. Moreover, it was interesting to note similar reports have been described for CNP synthesis. Masarudin et al. [33] has demonstrated the stability and dispersive nature of chitosan nanoparticles as candidate vector for anti-cancer drug delivery.

**Polydispersity index (pdi):** The term polydispersity index is used to describe the degree of “non-uniformity” of a distribution because it

facilitates understanding of dispersion and aggregation of particles in the medium. The size distribution of the phytofabricated nanoparticles as well as the chitosan nanoparticles are presented in Figure 5. The nanoparticles size distribution is reflected by the PDI values. The samples with higher range of particle exhibits higher PDI values while those consisting of lower range of particle exhibits lower PDI values. The result from the present study showed that the average size of prepared GSCNPs varies with a polydispersity index in the range of 0.474. The pdi values of chitosan nanoparticles (0.680) revealed that the particles obtained were heterogeneous in nature. It was reported that polydispersity index more than 0.5 is indicative to aggregation of particles [34]. The particle size of the nanoparticles was depending upon the molecular weight and concentration of the chitosan. The average size was smaller for the synthesized chitosan nanoparticles and GSCNPs in TEM analysis when compared to that measured by DLS system as described. These differences might be due to the measurement conditions and techniques used in the both the experiments as the principle was found to be different in both the cases. The variations in the chitosan nanoparticles swelling in aqueous media and DLS gave a hydrodynamic diameter of nanoparticles, while TEM showed an actual diameter of nanoparticles in dry state. Therefore, their structure was not in swelled stage resulting in lower size of the particles [35]. Similar

S. No	Characters	Properties
1	Particle size of the synthesized nanoparticles	Due to their unique size, the nanoparticles tend to own novel physical, chemical and biological properties that make these nanomaterials superior in the field of nanomedicine [10].
2	Stability	Depending on the polyelectrolyte ratio, the Zeta potential plays an important role in determining the stability of the synthesized nanoparticles [32].
3	Dispersive index	The polydispersity index value is used to determine the dispersion and aggregation nature of the nanoparticles synthesized in the medium [35] and analysed by the Dynamic Light Scattering technique.
4	Morphology	The surface and shape of the synthesized nanoparticles are important for the encapsulation of phytochemicals and is determined by the SEM, TEM techniques [30].

**Table 1:** Representation of the comprehensive properties of synthesized nanoparticles.

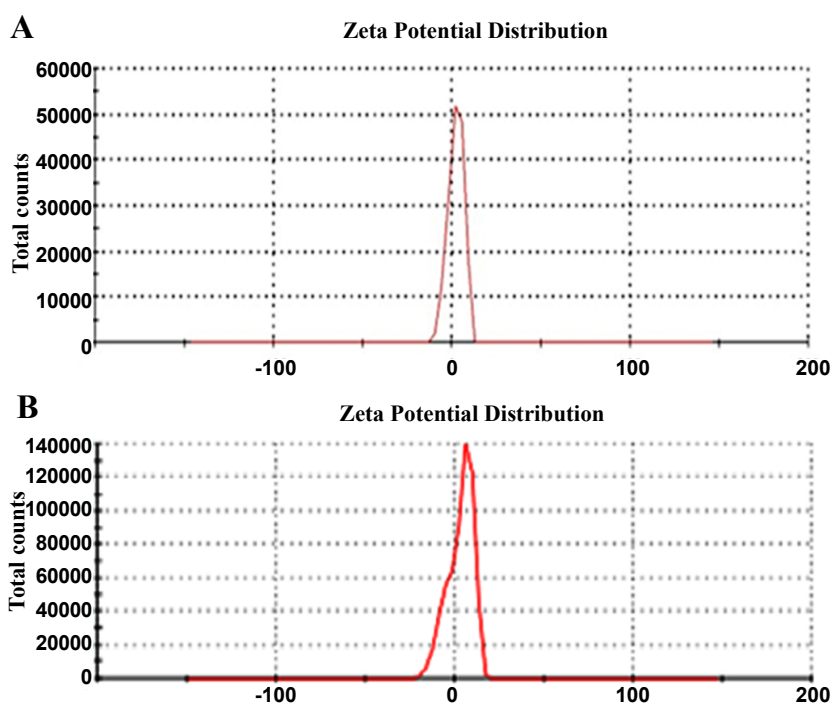


**Figure 4:** Zeta particle size distribution graph of A) Chitosan nanoparticles, B) *Gymnema sylvestre* leaf extracts derived phytochemicals cross-linked chitosan nanoparticles (GSCNPs).

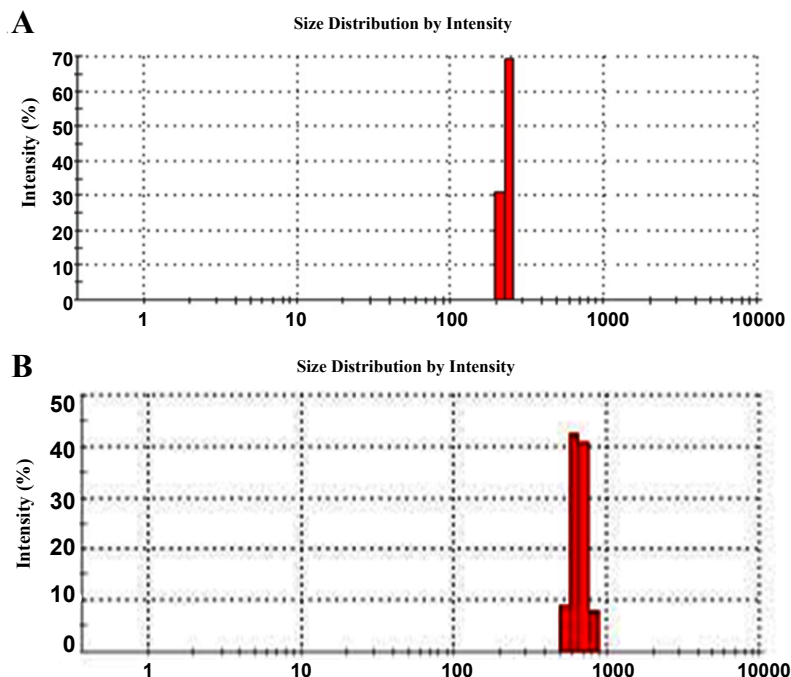


**Figure 5:** Particle Density Index results of A) Chitosan nanoparticles, B) *Gymnema sylvestre* leaf extracts derived phytochemicals cross-linked chitosan nanoparticles (GSCNPs).

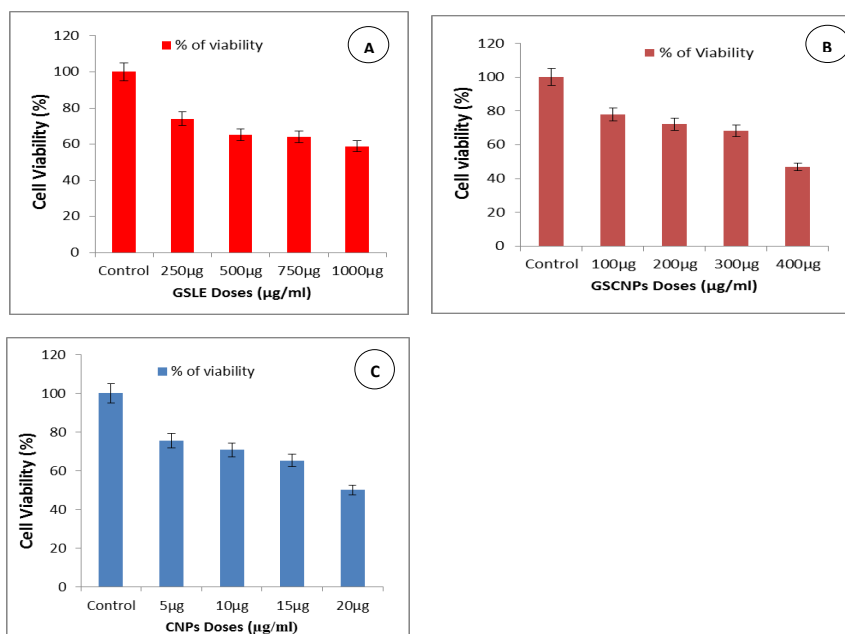


**Figure 6:** Cell viability of PA-1 cells treated with A) GSLE and B) GSCNPs C) CNPs at various concentrations for 24h and cytotoxicity was determined by MTT assay.

particle size distribution for the chitosan coated insulin nanoparticles with homogenous dispersion was reported by Avadi et al. [30].

**In vitro cytotoxicity of the synthesized nanoparticles:** The MTT assay, a widely used colorimetric based assay to detect the activity of mitochondrial dehydrogenase enzymes in cells is considered as a common methodology for the assessment of cytotoxicity in cancer cells [36]. In the present study, the *in vitro* cytotoxicity of GSLE and

GSCNPs were investigated against human ovarian cancer cell line (PA-1). The PA-1 cells were treated with different doses of methanol extract of *G. sylvestre* leaves (250 to 1000 µg/ml) and GSCNPs (100 to 400 µg/ml) for 24 h at 37°C. After treatment, the inhibitory percent of PA-1 cancer and normal 3T3 cell growth was determined. The percentage of cell viability obtained with continuous exposure for 48 h is depicted in Figure 6. The cell viability was also found to be decreased with increasing the concentrations of GSLE (Figure 6A) and GSCNPs (Figure 6B).

The cytotoxicity of NPs was found to be concentration dependent and the  $IC_{50}$  values were calculated using MTT assay. The assay was based on the reduction of soluble yellow tetrazolium salt to insoluble purple formazan crystals by metabolically active cells. Only live cells were able to uptake the tetrazolium salt. The enzyme (mitochondrial dehydrogenase) present in the mitochondria of the live cells was able to convert internalized tetrazolium salt to formazan crystals, which formed purple in color. Then the cells were lysed and dissolved in DMSO solution. The color developed was then measured in the ELISA reader at 570 nm. The  $IC_{50}$  dose was determined using Graph pad prism5 software. The  $IC_{50}$  values of PA-1 cancer cells were 931  $\mu\text{g/ml}$ , and 378.4  $\mu\text{g/ml}$  for GSLE and GSCNPs respectively. Results strongly showed the enhanced cytotoxicity of the synthesized GSCNPs at lower dose against the PA-1 cancer cell line than GSLE. The effect of NPs on the growth of normal cell lines (3T3 cells) did not exhibit significant cytotoxicity at their lower concentrations and cytotoxic activity increases with increased concentrations. The morphological changes in normal 3T3 cells and PA-1 cancer cells treated with GSLE and GSCNPs are represented in the microscopic images as shown in Figure 7. The most recognizable morphological changes observed due to the plant extract and nanoparticle treatments were cytoplasmic condensation, cell shrinkage, the production of numerous cells with surface bulges at the plasma membrane, and the aggregation of the nuclear chromatin into dense masses in PA-1 cells (Figure 7A-7C) while, both the GSCNPs and GSLE did not affect the normal 3T3 cell morphology

(Figure 7D-7F). Additionally, the cell membranes also became warped and changed to vesicle shape. It is interesting to note that GSCNPs treatment resulted in swelling and round morphology of cancer cells with condensed chromatin and the progressive structural modification as well as reduction in PA-1 cell populations when compared with the plant extract treated cells. The cellular uptake of nanoparticles was facilitated by the positive surface charge and interactions of chitosan-biomolecules complex. Thus the synthesized chitosan-nanocomplex showed stimulated cytotoxic activity against cancer cell growth because of the presence of saponin bioactive compound in the plant extracts, by reducing the required dose of nanodrug and leading to improved apoptotic activity. Similar morphological modifications were also described earlier by Sivalokanathan et al. [37] and Vivek et al. [38]. Earlier, Arunachalam et al. [39] also reported the role of bio functionalized *G. sylvestre* gold nanoparticles (GGNPS) against HT-29 cells treatment.

### Evaluation of caspase-9-activation

Apoptosis is generally considered as a complex activity that initiates more number of molecules that are classified into caspase-dependent or caspase-independent mechanisms. The activation of caspase is a crucial mechanism to apoptosis generally. To examine the molecular mechanism underlying apoptosis, the present study was involved in treating the PA-1 cells with HRP antibodies and Danisidine- $H_2O_2$  substrate of caspase for the determination of caspase-9 activity after treating with the desired samples. Further, the results were confirmed by the chemiluminescent assay and presented in Figure 8. It was observed that the PA-1 cells treatment with GSLE and GSCNPs induced dose dependent caspase activation in this study. The activity of caspase-9 was found to be increased gradually from the lowest concentration (50  $\mu\text{g/ml}$ ) and had obtained the peak in the highest concentration (200  $\mu\text{g/ml}$ ). It is noteworthy from the present study that the PA-1 cells treated with GSCNPs exhibited more caspase activity by inducing apoptosis compared to the GSLE treatment. The results on caspase-9 activity suggesting that the biomolecules loaded chitosan nanoparticles (GSCNPs) had significantly enhanced the cell death via apoptotic activity. It is reported that the release of cytochrome c from the mitochondria is mainly associated with the activation of caspase-9 [40]. A recent study also revealed the induction of apoptosis via the caspase pathway in human breast cancer cells [41].

### Comet assay for DNA fragmentation determination

The effect of GSLE and GSCNPs on DNA damage was determined by alkaline single cell electrophoresis (Comet Assay) based on the

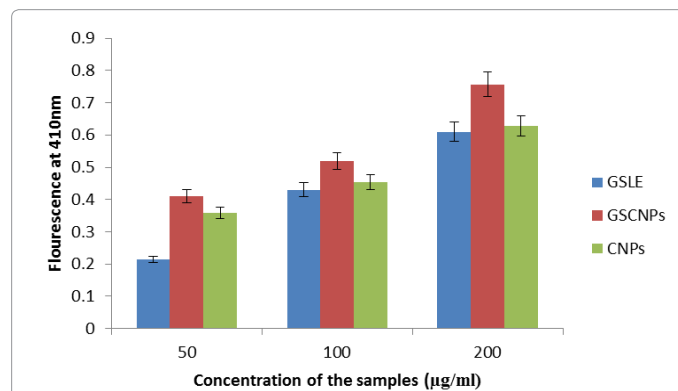
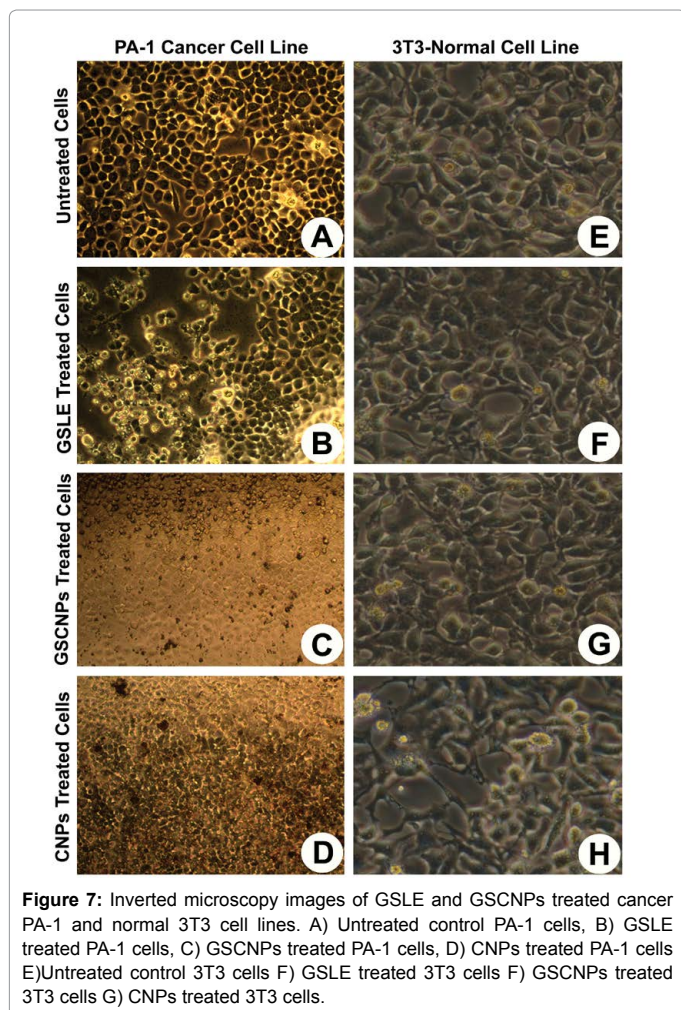


**Figure 8:** Determination of caspase-9 activation in PA-1 cells treated with GSLE, GSCNPs and CNPs.

ability of negatively charged fragments of DNA passing by agarose gel with support of an electric field. The extent of DNA migration directly depends on the DNA damage present in the cells. The present investigation has revealed a dose-dependent DNA damage in PA-1 cells. The results are illustrated in the Figure 9. Compared with the GSLE, the treatment of cancer cells with GSCNPs induced higher level of DNA damage at lower concentrations and is represented by the presence of DNA tail (Figure 9B). The increase in tail area and length reflects more extensive damages in the DNA of the treated cancer cells. From the Figure 10, it is evidently clear that the tail lengths were found to be increased with increasing the concentrations of the nanocomplex. Similarly, the genotoxic effect of *Artemisia nilagrlica* and *Murraya koenigii* extracts on mouse macrophage RAW264.7 cell line was also studied using comet assay [42].

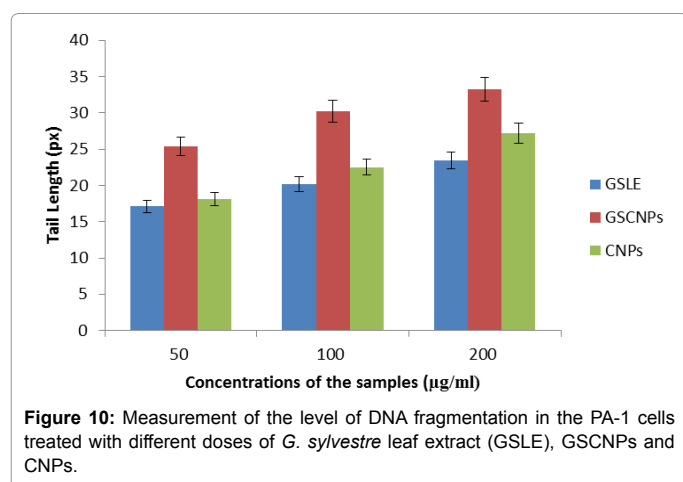
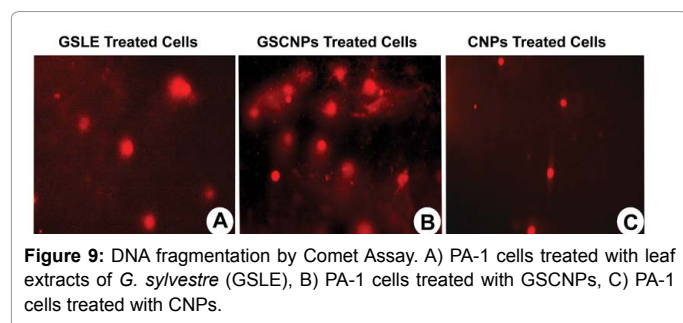
## Conclusion

In conclusion, an efficient protocol using the ionic gelation technique for the synthesis of phytochemicals cross-linked chitosan nanoparticles has been described in the present investigation. The synthesized nanoparticle was characterized by FTIR, XRD, TEM, Zeta potential and polydispersity index analysis. The crystalline nature and the functional group of the phytochemicals cross-linked chitosan nanoparticles were also studied. The synthesized nanoparticles were found to be spherical in shape with smooth surface. The zeta potential results confirmed the positive charges of GSCNPs and the homogenous distribution was proved by polydispersity index. The apoptotic potential of GSCNPs was studied against PA-1 human ovarian cancer cell line. Results strongly suggested that GSCNPs were found to be effective for enhanced cytotoxicity against the tested PA-1 cancer cells but did not affect the normal cells. Since the biomolecules encapsulated nanoparticles displayed potential ability, the finding of this study opens

up the possibilities for the treatment of ovarian cancer. This protocol may provide a platform for producing eco-friendly, non-toxic, and time consuming drugs for pharmaceutical industry that could be delivered appropriately in the future.

## References

1. Browne A, Sriraksa R, Guney T, Rama N, Noorden S, et al. (2013) Differential expression of IL-8 and IL-8 receptors in benign, borderline and malignant ovarian epithelial tumors. *Cytokine* 64: 413-421.
2. Osman MA (2015) Genetic cancer ovary. *Clin Ovarian Other Gynecol Cancer* 7: 1-7.
3. Korch C, Spillman MA, Jackson TA, Jacobsen BM, Murphy SK, et al. (2012) DNA profiling analysis of endometrial and ovarian cell lines reveals misidentification, redundancy and contamination. *Gynecol Oncol* 127: 241-248.
4. Yu J, Ma Y, Dristo J, Chen Q (2013) Antitumour activities of *Rauwolfia vomitoria* extract and potentiating of carboplatin effects against ovarian cancer. *Curr Ther Res* 75: 8-14.
5. Abulude FO (2007) phytochemical screening and mineral contents of leaves of some Nigerian woody plants. *Res J Phytochem* 1: 33-39.
6. Basu SK, Thomas JE, Acharya SN (2007) Prospects for growth in global nutraceutical and functional food markets: A Canadian perspective. *Aus J Basic Appl Sci* 1: 637-649.
7. Bone K (2003) A Clinical guide in blending liquid herbs: Herbal formulations for the individual patient. (1<sup>st</sup> edition) St. Louis, Churchill Livingstone.
8. Barbieri RL, Makris A, Randall RW, Daniels G, Kistner RW, et al. (1986) Insulin stimulates androgen accumulation in incubations of ovarian stroma obtained from women with hyperandrogenism. *J Clin Endocrinol Metab* 62: 904-910.
9. Nana A, Christine I, Sandberg WJ, Marcin MR, Brunborg KG, et al. (2012) Cytotoxic and genotoxic effects of silver nanoparticles in testicular cells. *Toxicol* 291: 65-72.
10. Wang Y, Xiao HE, Wang K, Zhang X, Tan W (2009) Barbated skull cup herb extract-mediated biosynthesis of gold nanoparticles and its primary application in electrochemistry. *Colloids Surf B: Biointerfaces* 73: 75-79.
11. Zhao LM, Shi LE, Zhang ZL, Chen JM, Shi DD, et al. (2011) Preparation and application of chitosan nanoparticles and nanofibres. *Braz J Chem Eng* 28: 353-362.
12. Malesu VK, Sahoo D, Nayak PL (2011) Chitosan sodium alginate nanocomposites blended with cloisite 30B as a novel drug delivery system for anticancer drug curcumin. *IJBAPT* 2: 402-411.
13. Mayyar MA, Al-Remauri (2012) Properties of chitosan nanoparticles formed using sulphate anions as cross linking bridges. *Am J Appl Sci* 9: 1091-1100.
14. Medina LS, Gomez AG, Ortega FR, Sousa IMO, Queiroz NDCA, et al. (2015) Chitosan-tripolyphosphate nanoparticles as *Arrabidaea chica* standardized extract carrier: synthesis, characterization, biocompatibility and antiulcerogenic activity. *Inter. J Nanomed* 10: 3897-3909.
15. Swarnalatha Y, Gunna GK, Jacob CM (2015) Synthesis of alkaloid loaded chitosan nanoparticles for enhancing the anticancer activity in A549 lung cancer lines. *Der Pharmacia Lett* 7: 378-390.
16. Manikandan A, Sathyabama M (2015) Green synthesis of copper-chitosan nanoparticles and study of its anti-bacterial activity. *J Nanomed. Nanotech* 6: 1-5.
17. Patel SI (2015) Chitosan nanoparticles synthesis from shrimp shell waste for application in the pharmaceutical industry. *IJSRE* 3: 2984-2994.
18. Albuquerque P, Coelho LC, Teixeira JA, Carneiro-da-Cunha, MG (2016) Approaches in biotechnological applications of natural polymers. *AIMS Mol Sci* 3: 386-425.
19. Mosmann T (1983) Rapid colorimetric assay for cellular growth and survival: application to proliferation and cytotoxicity assays. *J Immunol Methods* 65: 55-63.
20. Dhawan A, Bajpayee M, Pandey AK, Parmar D (2010) Protocol for the single cell gel electrophoresis/comet assay for rapid genotoxicity assessment. *ITRC* 1-10.
21. Kafshgari MH, Khorram M, Khodadoost M, Khavari S (2011) Reinforcement of chitosan nanoparticles obtained by an ionic cross-linking process Iran. *Polym J* 20: 445-456.



22. Liu H, Gao C (2009) Preparation and properties of ionically cross-linked chitosan nanoparticles. *Polym Adv Technol* 20: 613-619.
23. Lee DW, Lim C, Israelachvili JN, Hwang DS (2013) Strong adhesion and cohesion of chitosan in aqueous solutions. *Langmuir* 46: 14222-14229.
24. Gan Q, Wang T (2007) Chitosan nanoparticle as protein delivery carrier-systematic examination of fabrication conditions for efficient loading and release. *Colloid Surf B: Biointerfaces* 59: 24-34.
25. Rejinold SN, Muthunayanan M, Muthuchelian K, Chennazhi K P Shanthi VN, et al. (2011) Saponin loaded chitosan nanoparticles and their cytotoxicity to cancer cell lines in vitro. *Carbohydr Polym* 84: 407-416.
26. AbdElhady MM (2012) Preparation and characterization of Chitosan/Zinc oxide nanoparticles for imparting antimicrobial and UV protection to cotton fabric. *Int J Carbohydr Chem Article ID 840596*.
27. Talam S, Karumuri SR, Gunnam N (2012) Synthesis, characterization, and spectroscopic properties of ZnO nanoparticles. *ISR Nanotechnology* 1- 6.
28. Jingou J, Shilei H, Weiqi L, Danjun W, Tengfei W, et al. (2011) Preparation, characterization of hydrophilic and hydrophobic drug in combine loaded chitosan/cyclodextrin nanoparticles and in vitro release study. *Colloid Surf B: Biointerfaces* 83: 103-107.
29. Elsayed A, Al-Remawi M, Qinna N, Farouk A, Al-Sou'od KA, et al. (2011) Chitosan-sodium lauryl sulfate nanoparticles as a carrier system for the in vivo delivery of oral Insulin. *AAPS PharmSci Tech* 12: 958-964.
30. Avadi MR, Sadeghi AMM, Mohammadpour N, Abedin S, Atyabi F, et al. (2010) Preparation and characterization of insulin nanoparticles using chitosan and arabic gum with ionic gelation method. *Nanomed Nanotech Biol Med* 6: 58-63.
31. Al-Qadi S, Grenha A, Carrión-Recio D, Seijo B, Remuñán-López C (2012) Microencapsulated chitosan nanoparticles for pulmonary protein delivery: In vivo evaluation of insulin-loaded formulations. *J Control Release* 157: 383-390.
32. Raja MAG, Katas H, Wen TJ (2015) Stability, intracellular delivery, and release of siRNA from chitosan nanoparticles using different cross-linkers. *PLoS One* 10: e0128963.
33. Masarudin MJ, Cutts SM, Evison BJ, Phillips DR, Pigram, PJ (2015) Factors determining the stability, size distribution, and cellular accumulation of small, monodisperse chitosan nanoparticles as candidate vectors for anticancer drug delivery: application to the passive encapsulation of [14C]-doxorubicin. *Nanotech sci appl* 8: 67.
34. Bathool A, Vishakante GD, Khan MS, Shivakumar HG (2012) Development and characterization of atorvastatin calcium loaded chitosan nanoparticles for sustained drug delivery. *Adv Mat Lett* 3: 466-470.
35. Ali S W, Rajendran S, Joshi M (2011) Synthesis and characterization of chitosan and silver loaded chitosan nanoparticles for bioactive polyester. *Carbohydr Polym* 83: 438-446.
36. Ahmadi A, Mohagheghi MA, Karimi M, Golestanha SA, Naseri M (2009) Anticancer effects of HESA-A in patients with metastatic colon cancer. *Integr. Cancer. Ther* 8: 71-74.
37. Sivalokanathan S, Vijayababu MR, Balasubramanian MP (2006) Effects of Terminalia arjuna bark extract on apoptosis of human hepatoma cell line HepG2 *World. J. Gastroenterol* 12: 1018-1024.
38. Vivek R, Thangam R, Muthuchelian K, Gunasekaran P, Kaveri K, et al. (2012) Green biosynthesis of silver nanoparticles from Annona squamosa leaf extract and it's in vitro cytotoxic effect on MCF-7 cells. *Proc Biochem* 47: 2405-2410.
39. Arunachalam KD, Arun LB, Annamalai SK, Arunachalam AM (2014) Biofunctionalized gold nanoparticles synthesis from Gymnema sylvestre and its preliminary anticancer activity. *Int J Pharm Pharm Sci* 6: 423-430.
40. Garrido C, Galluzzi L, Brunet M, Puig P E, Didelot C, et al. (2006) Mechanisms of cytochrome c release from mitochondria. *Cell Death Differ* 13: 1423-1433.
41. Looi CY, Arya A, Cheah FK, Muharram B, Leong KH, et al. (2013) Induction of apoptosis in human breast cancer cells via caspase pathway by vernodalin isolated from *Centratherum anthelminticum* (L.) seeds. *PLoS One* 8: e56643.
42. Naik SK, Mohanty S, Padhi A, Pati R, Sonawane A (2014) Evaluation of antibacterial and cytotoxic activity of Artemisia nilagirica and Murraya koenigii leaf extracts against mycobacteria and macrophages. *BMC Complem. Altern Med* 14: 10.